Following excited states in molecular systems using density-based indexes: A dual emissive system as a test case

Anna Perfetto, Federica Maschietto, Ilaria Ciofini

Following excited states in molecular systems using density-based indexes: a dual emissive system as a test case

Anna Perfetto[#], Federica Maschietto[#], Ilaria Ciofini[*]

Chimie ParisTech, PSL University, CNRS, Institute of Chemistry for Life and Health Sciences, Theoretical Chemistry and Modelling, 75005 Paris, France.

# These authors have contributed equally to the present work.

*Email: ilaria.ciofini@chimie-paristech.fr

ORCID-ID:

Anna Perfetto: 0000-0002-8145-7197
Federica Maschietto: 0000-0002-5995-2765
Ilaria Ciofini: 0000-0002-5391-4522

Abstract

Dual emission from single molecular species is a particularly appealing phenomenon to test the efficiency of theoretical approaches for the description of a complex excited state scenario.

Recently, the Phen-PENMe$_2$ molecule (Phen-PENMe$_2$ = 5-(4-dimethylaminophenylenylethylyn)-1,10-phenanthroline) has been experimentally characterized and its dual emission has been ascribed to the presence of two emissive states of different electronic nature and corresponding to two structurally different species. Nonetheless, the full mechanism ruling the structural interconversion leading to dual emission has not yet been disclosed.

To this end, in this paper the dual emissive behavior of Phen-PENMe$_2$ has been unveiled by a combined use of time dependent density functional theory (TD-DFT) and density-based indexes (D_{CT} and Π) allowing identifying the radiative and non-radiative decay pathways at work in this system. In particular, the presence of an anti-Kasha emission mechanism as well as the presence of several non-radiative decay channels allowing enhancing either of the two emissions has been proven.

More generally, the results obtained in the present study highlight how this simple and inexpensive computational approach may be of help and general interest for the rational design of new dual emissive systems.

Keywords:

Density-Based Index; Dual Emission; Excited State pathway; Density Functional Theory;

1. Introduction

Dual emission in molecular systems is a phenomenon increasingly reported in the literature and attracting ever-growing interest.[1-6] Depending on the mechanism at the origin of dual emission, various classes of compounds may be identified. Indeed, widely documented is dual fluorescence occurring in small organic dyes undergoing excited state intramolecular proton transfer (ESIPT) reactions[7-14] or excited state intramolecular charge transfer processes.[3,15-21]Such dual emission phenomena have been exploited in the synthesis of various novel chemosensors with different target applications.[7,8,10,22] Dual emission through Thermally Activated Delayed Fluorescence (TADF) deserves of being explicitly mentioned.[1,2,5,6,23-25] These systems are indeed regarded as promising next-generation organic electro-luminescent materials due to their potentially high internal quantum efficiency.

Beside their relevance for applications, molecules displaying dual emission provide a perfect playground to test and validate theoretical approaches aiming to investigate the structural and electronic features of excited states yielding both to radiative[26-27] and non-radiative[9,15,28-30] decay pathways. Indeed, besides molecular systems where dual emission is associated to a change in the chemical nature of the emitting specie (ex. protonation state),[7,8-10,12-] native dual emission is usually associated to the presence of two emissive -bright- excited states of different character that can be both populated and that are stabilized by a differential structural reorganization.

In this respect, theoretical approaches aiming at describing this kind of phenomena are of great interest. There are at least two criteria that a method shall fulfill in order to deliver a good understanding of photochemical processes. Firstly, it should reproduce correctly the potential energy surfaces (PES) of the excited states of interest, within and far from the Franck Condon (vertical excitation) region. Next, it should deliver a coherent picture of the photochemical process from the absorption to the emission.

Ab-initio excited state dynamic approaches[26,30-32] can provide this type of information but are often expensive for a routine analysis. By contrast, a static study of the PES as the one proposed in the present study may provide a simplified picture of the possible decay channels in play, delivering a realistic, yet qualitative understanding of the whole process at an affordable computational cost.

In this work we use density-based descriptors to follow the evolution of excited states along a given reaction coordinate, with the aim of proposing a strategy to rationalize the mechanism

of the dual emission phenomena in Phen-PENMe$_2$ (Phen-PENMe$_2$ = 5-(4-dimethylaminophenylenylethylyn)-1,10-phenanthroline).

Indeed, from a theoretical point of view, a large number of studies,[5,14,19,33-36] including our previous ones[15,17,27,37-39] has focused on the description of the excited states using density-based descriptors to analyze the nature of the excited states responsible for the observed absorption and emission, both from a structural and energetic point of view. For a recent and complete review see for instance reference.[40] To this end, in the last years, we introduced some strategies for the description of excited states, coupling Time-Dependent density functional theory (TD-DFT) with descriptors based on electron density.[27,41-43] This type of indexes were primarily aiming at the diagnostic and description of excited states with a charge-transfer character, with the use of the so-called $D_{CT,}$ acronym of Distance of charge transfer and M_{AC}, acronym of Mulliken averaged configuration.[43-45] Recently a new index - so called Π - was also developed enabling to qualitatively identify excited-state potential energy regions where decay channels (both radiative or non-radiative) are highly expected. Unlike previous density descriptors, the Π index provides an estimate of the probability of different electronic states to interconvert, thus allowing to map the evolution of an excited state along a reaction coordinate. Up to now, this approach has been tested to explore simple photochemical processes, such as ESIPT or to analyze the excited states PES of prototype dual emissive systems such as the 4-N,N-dimethylaminobenzonitrile molecule (DMABN).[45]

In the present work, we apply this strategy to study the photophysical behavior of Phen-PENMe$_2$ here considered as a complex but experimentally well-characterized example of a single dual-emissive molecule.[15,16] To this end, we explored by the mean of the Π index, all its possible decay pathways thereby providing a deeper understanding of the electronic origins of the observed dual emissive behavior.

The Phen-PENMe$_2$ can be considered as a typical push-pull system thus similar to many dual emissive molecules relying on a Donor-π bridge-Acceptor structure (D-π-A),[17] starting from the pioneering DMABN[46] system, to more recently synthesized systems possessing stilbene,[47] pyrene,[13] imidazole,[19] or 9-aminoacridine[22] or dimethylamino-phenyl-penta-2,4-dienoic acid ethyl ester (DMAPPDE) skeletons.[20] The Phen-PENMe$_2$ molecule is composed of a 1,10-phenanthroline core (*Scheme 1*) functionalized with a dimethylaminophenyl group acting as an electron donor.

Recent combined experimental and theoretical studies performed by some of us[15,16] clarified that the observed dual emission is associated with the existence of two different emissive states: a planar Intra-Molecular Charge Transfer (ICT) state corresponding to an electronic

transition from the donor moiety to the phenanthroline core, and a Locally Excited (LE) -state centered on the 1,10-phenanthroline, in which the donor and acceptor are orthogonally oriented. These earlier experimental and theoretical studies also investigated the solvent dependence of the dual emission phenomenon and highlighted the importance of the use of polar-aprotic solution to allow for the formation of both conformations, thus yielding the dual emission.

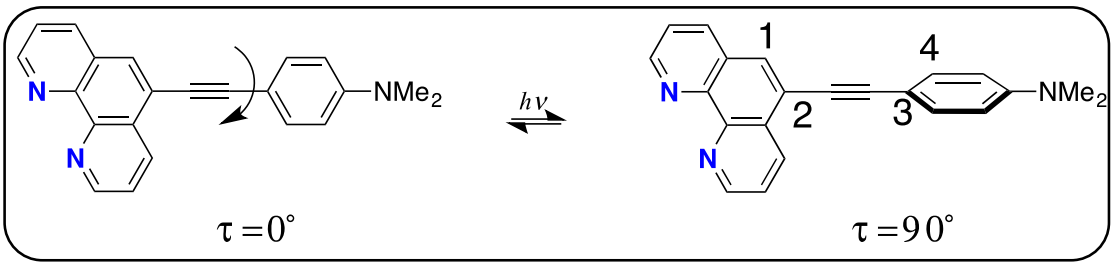

Scheme 1. Schematic structure of the Phen-PENMe$_2$ molecule in its planar (τ=0°) and twisted conformations (τ=90°).

If the nature of the emissive states has been disclosed,[15,16] the pathways connecting the excited states initially populated in absorption to the ones that actually emit has not yet been thoroughly analyzed. This is the question we aim to answer in this work, using density-based descriptors.

The paper is organized as it follows. In *Section 2* we briefly introduce the density descriptors and quantum methods applied. In the *Section 3* we provide the reader with a general description of the excited states responsible for the peculiar photochemical behavior of Phen-PENME$_2$, through a simple analysis of the energetics, and of the nature of the vertical electronic transitions. These two simple elements are very informative and deliver an approximate -yet coherent- picture of the process, though missing some crucial features. Further on, we investigate the same process using the Π index. This descriptor combines the information delivered by the energy and the D_{CT} into a more elaborate function, giving access to additional knowledge on the excited state decay pathway. As a result, we identify a number of decay channels, and rationalize, the photochemical behavior of Phen-PENMe$_2$ from the vertical absorption to the emission. Finally, in the last section we draw some general conclusions.

2. Computational details and density-based indexes

In previous experimental and theoretical works[15,16] we showed that two structurally distinct forms, differing by the orientation of the phenyl and phenanthroline rings are responsible for the observed dual emission. The reaction coordinate connecting these two forms is the

dihedral angle $C_1C_2C_3C_4$ (see *Scheme* 1) which we refer to as τ in the following. We performed a relaxed scan starting from the ground state - planar - optimized structure by varying τ from 0° to 90° in increments of 10°. The resulting ten geometries encompass the full transformation from the planar to the twisted (perpendicular) structure. Excited states were computed vertically on top of each structure. In line with previous works on the same system,[16] all computations were performed at density functional theory (DFT) and TD-DFT[48-49]level, respectively for the ground (GS) and excited states (ES), and applying the CAM-B3LYP range-separated hybrid exchange-correlation functional,[50]in combination with the 6-311+G (d,p) basis set.[51]

Of note, the CAM-B3LYP functional have proven to provide reliable ES-PES and have been specifically validated in the case of push-pull system giving rise to twisted conformations at the excited state (which is also the present case), see for instance the work of Tozer et al.[52] and Adamo et al.[53] Solvent effects (here acetonitrile) were taken into account employing the polarizable continuum model (PCM), in its conductor-like version (CPCM)[54] using a linear response (LR) scheme. An extensive literature is available on the comparison between State Specific (SS) and LR schemes for the evaluation of solvent effect on both CT and LE states see for instance ref. 55. Nonetheless the computationally less expensive LR scheme has been here applied on the basis of the results obtained in a previous benchmark, showing that the present computational protocol is able to correctly reproduce the experimental absorption and emission profiles - recorded in polar aprotic solvents for the present molecule.[15,16] All calculations were performed with the Gaussian16 software.[56]

To characterize the nature and the evolution of the excited states, we computed both the D_{CT} and the Π indexes all along the reaction coordinate. A detailed description of the indexes mentioned above is provided in the literature.[27,42-43,45]For ease of reading, here, we briefly recall their basic formulation. The D_{CT} quantifies the length of the hole-electron separation associated with a given electronic transition and therefore provides an estimate of the spatial extent of a given electronic transition, allowing to monitor the changes in the character of the excited states (for instance Locally Excited –LE versus Charge Transfer –CT-). This index is calculated as the module of the distance between the barycenters (R_+ and R_-) of the charge density corresponding to the hole and particle.

$$D_{CT} = |R_+ - R_-|.$$

Positive and negative barycenters are obtained by integration of the associated electron densities, ϱ^+ and ϱ^-. These last are derived from the difference in total density of the two states S_i, S_j involved in the electronic transition - where $i, j = 1, \ldots, n \in R$.

The Π index broadens the information provided by the D_{CT}, by coupling this last both with a charge displacement and an energetic term. It is correlated to the inverse of the work needed to accomplish the charge rearrangement associated to an electronic transition from one electronic state to another. Therefore, it can be used to identify, in a qualitative manner, regions of the excited state potential energy surfaces where decay pathways are more likely to occur. Indeed, in the case of two classical point charges q^+ and q^-, with a displacement vector (r) pointing from the negative charge to the positive charge, the electric dipole moment is given by

$$\mu = r \cdot q$$

Analogously in a molecule, the dipole moment produced in any S_i to S_j transition is given by the product between the negative - or positive - transferred charge and the sum of all the position operators of all the electrons in the molecule. The norm of the difference in the dipole moment of two electronic states *i* and *j* is given by:

$$\Delta\mu_{ij} = \| \mu_i - \mu_j \|$$

One can expand $\Delta\mu_{ij}$ as a function of the actual hole-particle transferred charge (hereafter q_{CT}) and the charge separation length associated with the given electronic transition (D_{CT}).

$$\Delta\mu_{ij} = q_{CT} \cdot D_{CT}.$$

Combining this product with the energy gap ΔE, the Π is readily obtained as,

$$\Pi = \frac{1}{\Delta E \cdot q_{CT} \cdot D_{CT}}.$$

High values of Π will thus define the regions corresponding to the higher decay probability. Although the energy gap between the two states is generally the most relevant term for many photochemical reactions implying a crossing of states, for a given energy gap, a decay between two states will be more efficient depending on the similarity between the electronic densities of the starting and final states. In other words, the smaller the reorganization of the electronic distributions between the two states, the greater the probability of decay. Therefore, efficient decay pathways are likely to emerge in regions where two states are close together in energy ($\Delta E_{ij} \rightarrow 0$), when the electron densities of two states are similar ($\|\mu_{CT}\| = D_{CT} \cdot q_{CT} \rightarrow 0$), or when both of these criteria occur simultaneously. The Π index combining both

information coming from the dipole moment and the energy difference provides therefore a more complete description with respect to each of its constituting components.

D_{CT} and Π index values have been evaluated using an in-house developed and freely available code.[57] Absorption spectra are simulated by Gaussian convolution of the computed vertical transition energies using a full width at half maximum (*fwhm)* value of 0.2 eV.

3. Results and discussion

To investigate the photophysical behavior of the Phen-PENMe$_2$ molecule we have analyzed the evolution of the ground state and of the first six excited states, along the coordinate of interest (in *Scheme 1*). This last involves the formation of a planar and an orthogonal conformer, which differ in the orientation of phenyl and phenanthroline rings.

Ground state DFT calculations computed at each reaction step revealed a rather flat ground state potential curve. The planar structure (τ=0°) is the minimum, though only by 0.04 eV (1.45 Kcal/mol) lower in energy compared to the orthogonal conformation (τ=90°), the maximum of the ground state curve.

Excitation in the 3.5-4.0 eV (354-310 nm) energy regime, populates the first excited state (S_1). All along the reaction coordinate, the potential energy curve of S_1 (in yellow in the upper panels of *Figure 1*) increases monotonically, without any crossing over other excited states curves. The absorption is most efficient in the Franck-Condon region - where the oscillator strength is maximal (1.60 a.u.) - and decreases ceaselessly, down to a value of 0.0 a.u. for the twisted conformation (τ=90°).

Figure 2, showing the normalized Boltzmann distributions of each state, points out to similar conclusions. Indeed, the ground state appears to be equally populated at all reaction steps, while the first excited state S_1 is only accessible in the $0° < \tau < 20°$ region. As a remark, conventional DFT functionals tend to overestimate the strength of π - conjugation, with a consequential flattening of the ground state profile,[58] and deprecation of the GS Boltzmann population, though by using a range separated hybrid we mitigate this effect.

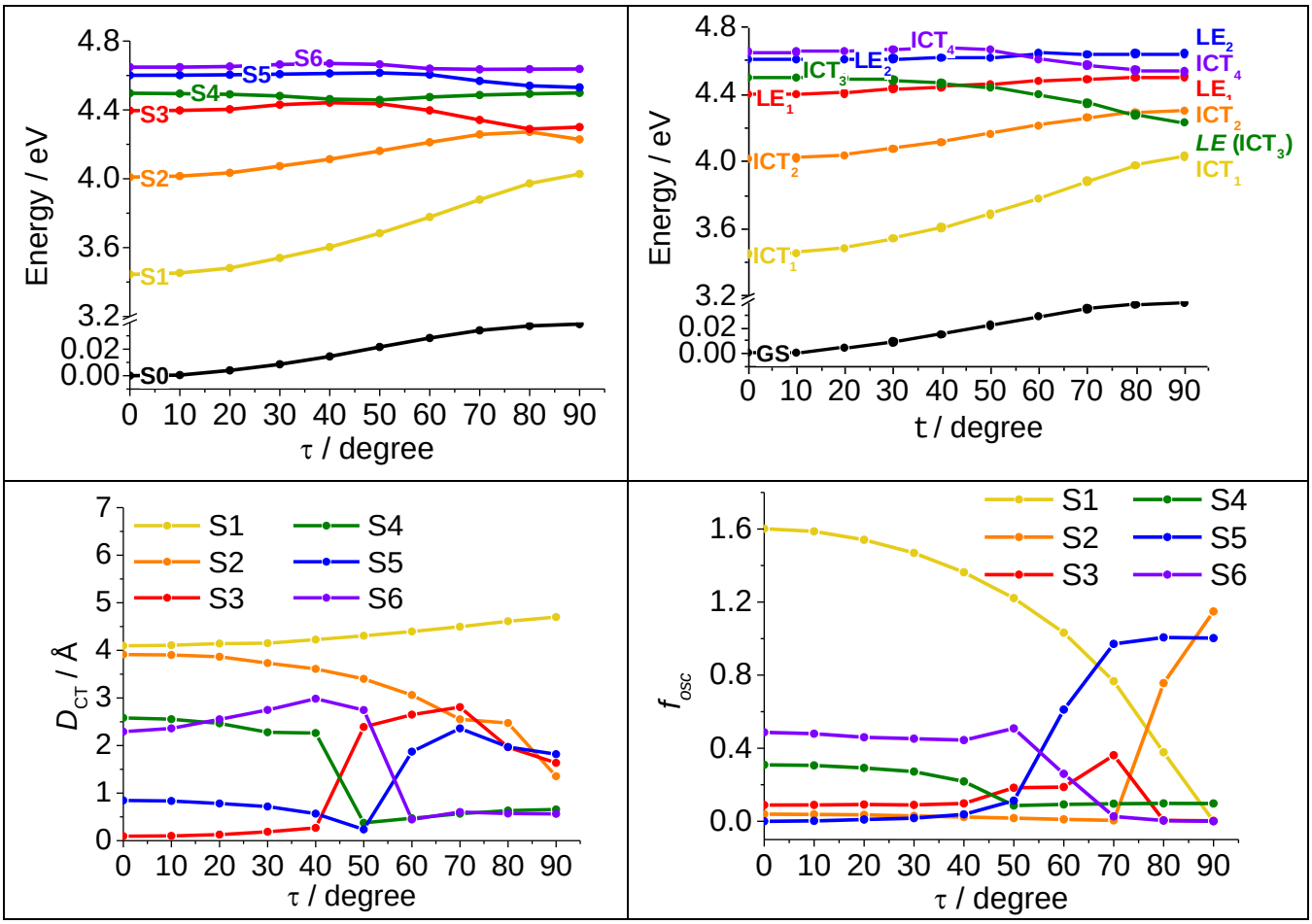

Figure 1 Upper panels: Ground (S_0) and first excited states (S_1-S_6) computed energy profiles (in eV) along the τ torsional degree of freedom. Upper-left panel: the excited state labels follow the energy indexing at τ = 0°; upper-right panel: the excited state labels are assigned according to their nature at τ = 0°. Lower panels: computed D_{CT} (in Å) and oscillator strength (f_{osc}, in a.u.) associated to each excited state, labelled according to the energy.

To identify the local or non-local character of each state, we rely on the computed D_{CT} values.[42] S_1 possesses a charge-transfer character, as indicated by the large D_{CT} values all along the reaction coordinate - ranging from 4.096 Å (τ = 0°) to 4.699 Å (τ = 90°). Accordingly, the two main-contributing natural transition orbitals (NTO) (in Supporting Information) occupy two spatially different regions: the hole-orbital localizes on the dimethylaminophenyl donor fragment, while the particle sits on the phenanthroline as expected for a donor to acceptor transition.

The marked CT character may also be inferred by the significant dipole moment variation computed for the S_1-S_0 transition (~12 Debye at τ = 0°). Consistently, the D_{CT} is indeed related to the norm of the difference in dipole moment $\Delta\mu_{ES\text{-}GS}$.[42]

Irradiation at 4.0-4.2 eV (309-293 nm) allows the second excited state to be accessed (orange curve in upper-left image in *Figure 1*). The energy profile of S_2 increases in energy until it reaches its maximum and approaches the third excited state at about $\tau = 80°$. At this point, we have the choice to analyze the energy profiles either according to their placement relative to the ground state curve or according to the nature of each excited state. This duple representation (shown in the upper left and right panels of *Figure 1*), turns out to be a handful approach, precisely to follow the evolution of the excited states, condensing the information provided by different observables - energy D_{CT}, and oscillator strength (f_{osc}) - in a unique picture. The Boltzmann population curves (*Figure 2*) are also labeled according to the nature of the states.

The D_{CT} profile computed for S_2 ranges from 3.913 Å at $\tau = 0°$ to 1.355 at $\tau = 90°$, denoting a change in nature from a charge-transfer state to a locally excited one. Accordingly, the $\Delta\mu_{ES\text{-}GS}$ decreases by one order of magnitude, converging towards the ground state value (10 Debye at $\tau = 90°$). Besides, S_2 changes from a dark state at $\tau = 0°$ ($f_{osc} = 0.039$) to a bright state at $\tau = 90°$ ($f_{osc} = 1.148$).

S_3 (red curve in the upper-right panel of *Figure 1*) is only accessed irradiating at energies higher than 4.4 eV (289 nm). Also, this excited state approaches both S_4 and S_2 at $\tau \sim 30°$ and $\tau \sim 80°$ respectively. According to *Figure 2*, the population of S_3 (LE_1), decreases considerably, going from 0° to 90°, while the opposite occurs for S_4.

As a result, one may infer that a crossing involving S_4 and S_3 occurs around $\tau = 30°\text{-}40°$. This inversion also appears in the D_{CT} profiles, where the S_4 and S_3 curves cross, pointing out a change in nature of the two states. In the $\tau = 0°$ to $\tau = 40°$ window, S_4 has a marked CT character, which translates in D_{CT} values ranging from 2.581 to 2.262 Å. S_3, on the other hand, exhibits small D_{CT} values, synonymous of a localized transition (0.1-0.2 Å).

At $\tau \sim 50°$, the picture is inverted. Here, the fourth excited state localizes on the dimethylaminophenyl fragment - the D_{CT} value drops to 0.374 Å while S_3 takes over the CT character (2.388 Å). At this stage, S_4 remains unvaried till the completion of the twist, while S_3 approaches S_2 close to $\tau \sim 80°$. The CT length decreases for both S_2 and S_3 states to ~ 1.5 Å for the fully twisted conformation. As we will discuss later on, the S_4-S_3 inversion is the critical step to access the dual emission.

The photochemical pathway outlined results in the population of the S_4 state. In summary, S_3 acts as a bridge between S_4 - bright CT state in the FC region - and S_2, LE state - initially dark, and turning into a bright state around 80°. The NTOs, available in Supporting

Information, render an orbital picture of the changes in nature of the corresponding electronic transitions.

Finally, the higher excited states, S_5 and S_6, require respectively excitation energies of 4.60 eV (269 nm) and 4.65 eV (267 nm) to be populated. The corresponding D_{CT} curves cross around $\tau = 55°$, suggesting an inversion in their character. S_5 approaches then the trajectory of S_4 at $\tau \sim 90°$. The latter, though, lies ~ 0.2 eV above S_3, limiting the mixing with the lower lying states. S_6 (ICT_4), however, appears to be populated between 50° and 90°, suggesting that it may contribute to feeding a non-radiative channel transferring its population to the lower states. It is worth recalling that, due to the very low energetic barrier, at the GS the molecule is able to freely rotate, hence all conformations are accessed. Irradiating the molecule at low energies limits the access to the excited state levels to the sole S_1. This, in turn, prevents the twisting and with it the formation of the *LE* state, thereby leading to a single emission from the planar ICT_1 (S_1). By contrast, exciting with sufficient energy, all excited states may be reached, leading to a multitude of decay pathways.

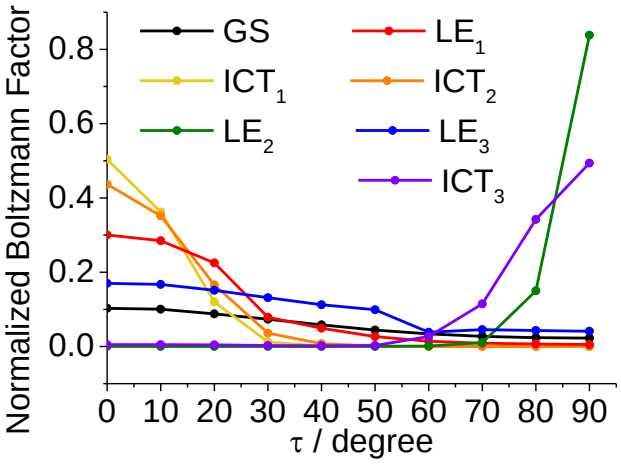

Figure 2 Computed normalized Boltzmann factors (computed at T=298 K for each state) for the ground state and first six excited states (labelled as a function of their nature, *Figure 1* upper-right panel) as a function of τ dihedral angle. Each curve is normalized w.r.t. its maximum value.

3.1 Simulation and interpretation of the observed absorption spectrum

Before analyzing in details the decay pathways it is useful to comment on the absorption properties of Phen-$PENMe_2$, as such analysis will later be helpful to disclose the mechanism leading to the dual emission.

The simulated absorption spectrum at each internal conversion coordinate (in *Figure 3*) reflects the vanishing of the ICT_1 state and rising of the *LE* / state as the molecule twists. In

the planar conformation (τ = 0°), the absorption is dominated by a single transition at 355 nm (3.49 eV). The resulting broad absorption band is ascribed to the lowest excited state, S_1 (ICT_1), of CT character. The band at 270 nm (4.59 eV) arises from two higher ICT states - S_4 and S_6 - and, to a smaller extent, from an LE state of nπ* character (S_3). Despite the low oscillator strength of the states involved - they are not exceeding 0.5 a.u. at 0° - the band appears intense, as the three states involved (S_3, S_4, and S_6) are relatively close in energy.

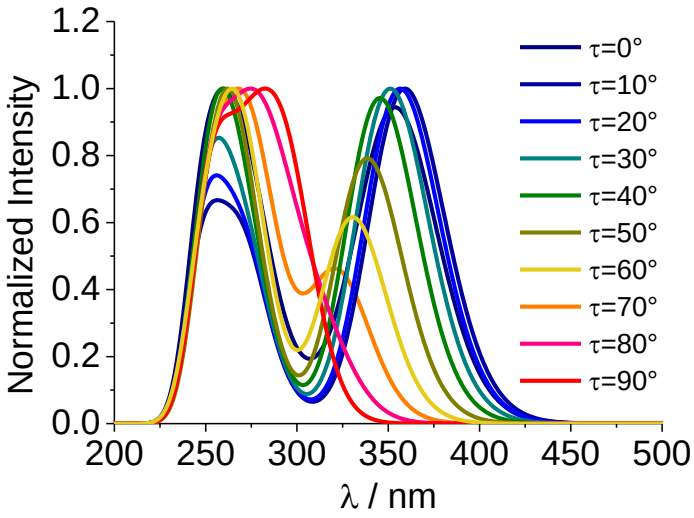

Figure 3 Absorption spectrum of Phen-$PENMe_2$ at fixed dihedral angles, ranging from 0° to 90°simulated by Gaussian convolution of the computed vertical transition energies using a fwhm value of 0.2 eV. The color-coding highlights the raising and vanishing of the LE and ICT_1, respectively.

At (τ = 90°), the absorption spectrum consists of a single band at 296 nm (4.19 eV) - with a shoulder at higher energy (276 nm / 4.49 eV). This band is ascribed to transitions involving two states: a LE state (S_2) of $\pi\pi$* character centered on the 1,10-phenathroline fragment and an ICT state (S_5).

The absorption spectra computed at intermediate values of τ smoothly connect these two limiting pictures. The lowest energy band blue-shifts as the molecule twists and disappears entirely at $\tau \sim 90°$. At the same time, the highest energy band rises, while increasingly red-shifting.

The effect of the solvent in Phen-$PENMe_2$ was investigated previously.[15,16]

Considering the ground state PES of Phen-$PENMe_2$ computed in acetonitrile we can estimate that the molecule freely twists so that each conformation can contribute to the absorption.

Therefore, it is convenient to estimate an average absorption by pondering each of the spectra – calculated at different values of τ - using their corresponding GS Boltzmann weights. The outcome is shown in *Figure 4*. The band around 350 nm (3.54 eV) is the result of the ICT_1 (S_0

to S_1) transition. The highest energy band at 265-295 nm (4.68-4.20 eV) arises from the convolution of mainly two different states, whose contribution is highlighted with a blue background in the simplified Jablonski diagram reported on the right hand of *Figure 4*. The transitions lying between 280 and 295 nm (4.43 and 4.20 eV) correspond to the evolution of the ICT_3 ~~ICT_2~~ state, stemming from the S_0-S_4 transition in the $0° < \tau < 40°$ window. The same state is then populated by S_0-S_3 transition at dihedral values between 40° and 70°, and by S_0-S_2 transition at $70° < \tau < 90°$. Slightly higher in energy, at 280-270 nm (4.43-4.59 eV) the S_0-S_4 ($0° < \tau < 60°$) and S_0-S_5 transition ($60° < \tau < 90°$) sum up with the other closely lying transitions to contribute to the second band.

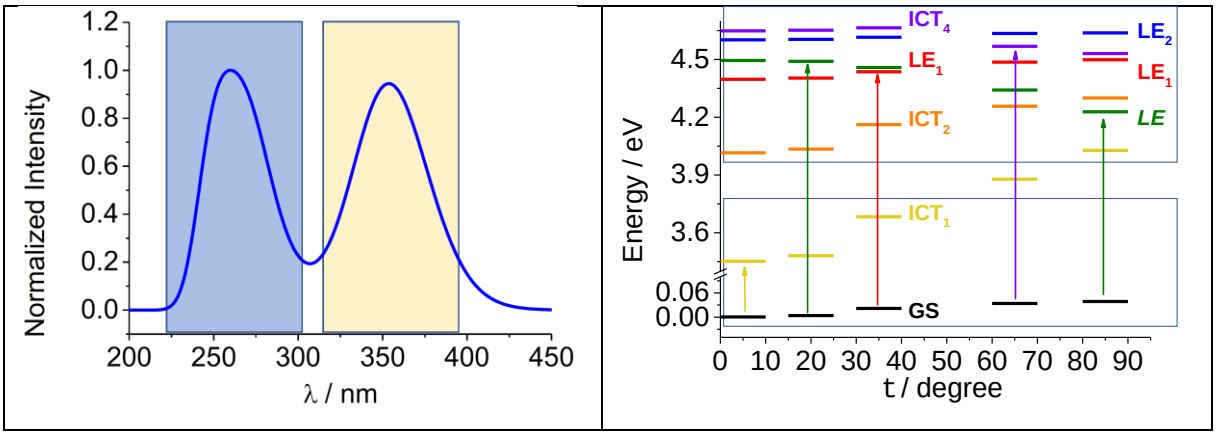

Figure 4 Left: Boltzmann weighted simulated absorption spectra of Phen-$PENMe_2$ Right: Jablonski diagram describing the absorption phenomena occurring in the Phen-$PENMe_2$ molecule.

3.2 Interpretation of the dual emission through the Π index

Up to now, we have used a combination of several observables, each bearing a different physical meaning, to sketch a map of the excited state pathways from the absorption region to the emitting one. Also, we have postulated the existence of several decay channels. However, to reach the correct interpretation, it is essential to assess the relative importance of each. To answer this question, the Π index will here be used. It is important to mention though that the methodology we are about to discuss is based on static considerations. Therefore, it does not give any indication on the time-scale of the photochemical process. As a result, any consideration on the kinetics of the electronic process remains out of our scope.

As previously mentioned, the Π index combines energetic arguments - ΔE - and a measure for charge rearrangement - $D_{CT}{\cdot}q_{CT}$ - and can be used as criteria to detect the presence of non-radiative decay channels. It is useful to compare the relative value of the Π index between electronic transitions that involve a common electronic state. This approach provides a

reasonable estimate of the relative likelihood of the existence of a decay channel, connecting more efficiently an electronic state with one or another state, lower in energy. Intuitively, this information shall be coupled with the vertical absorption, in order to map the excited states all through the pathway that brings to the emission. As for this aspect, a radiative relaxation yielding an emission from any excited state S_n necessarily implies that this particular state of interest is populated either directly, by irradiation, or by decay from an energetically higher excited state. The Π index, combined with the absorption data, provides precisely this information, thereby allowing to estimate the relative efficiency of the relaxation pathways connecting any two states all along a reaction coordinate. The result is a qualitative strategy, which delivers a consonant interpretation of a photochemical process, in an uncomplicated manner. Besides, the Π index is also computationally inexpensive, which is often not the case when one uses alternative approaches to deal with such questions. Undoubtedly, the global understanding of the physical phenomena will strongly depend on the quality of the ground, and excited states computed PES and thus will be affected by the level of theory (method and basis set) used to calculate densities and energies. This said, the level of theory which we have used to perform our calculations was chosen based on the result of a previous benchmark, which proved to give a good agreement with experimental data, both for absorption and emission. More details are provided in *Section* 2.

The Π index curves - in logarithmic scale - are reported in *Figure 5* (left panel). We recall that high values of the Π index correlate with a high probability of interconversion from a state to another.

Two regions of decay result unequivocally. The first is the S_4 to S_3 decay, appearing around $\tau = 40°$ in the solid olive-green curve. The second connects S_3 and S_2 and is indicated by the marked increment of the Π index associated with the S_3-to-S_2 transition between $\tau = 60°$ and $\tau = 90°$. These two curves allow identifying a leading non-radiative decay channel connecting S_4 to S_2 via S_3. This decay pathway is essentially energy-driven, i.e., it is promoted by the energy nearness of the three states, at specific reaction coordinates. This channel corresponds to the S_4-to-S_2 decay pathway that we had anticipated earlier through the energetic analysis (refer to *Figure 2* and related discussion).

The case of those decay channels that are governed by the product $D_{CT} \cdot q_{CT}$ is subtler. The analysis of *Figure 5* suggests the existence of two further decay and emission channels at $\tau = 0°$ and $\tau = 90°$. In the right panel of *Figure 5*, we collected the Π curves relative to the S_n-S_0 transitions, weighted by their corresponding oscillator strength. As the oscillator strength is

directly proportional to the transition probability, weighted-Π values provide a better estimate of the existing emission channels.

The largest weighted-Π value appears at $\tau = 0°$ and is associated with the S_3-S_0 transition (see right side of *Figure 5*), followed, in the same region by the S_1-S_0 transition. The observed shapes of the S_3-S_0 and S_1-S_0 curves suggest that the LE ($\pi\pi^*$) state, corresponding to S_3, together with the ICT_1 state (S_1) are likely to be primarily responsible for the emission in the Franck-Condon region. Additionally, the computed Π profiles point out an efficient interconversion between S_2-S_1 (solid orange curve) and a non-negligible interconversion between S_3-S_2 (solid red curve) that transfer the electronic population to the lowest excited state. We conclude that the ICT_1 emission is compliant with Kasha's rule. Although both S_3 and S_1 may be populated upon absorption, only the S_1 emits, and the S_3-S_2 and S_2-S_1 non-radiative decays enhance this emission channel. These outcomes agree with the experimental data substantiating the existence of an efficient ICT_1 radiative channel.[15,16] The vertical deactivation pathway transferring the electronic population from S_4 to S_1 (through the S_3-S_2-S_1 decay channels) and leading to the ICT_1 emission, is poorly efficient compared to the relaxation pathway activated by the torsion. As anticipated earlier in the discussion, if the molecule is irradiated with sufficiently high energy one activates the structural relaxation, which in turn results in populating (*LE*) S_2 state at 90°. The pathway involves the conversion between state S_4 to state S_3 (at around 50°) followed by the conversion of S_3 to S_2 at ~ 80°.

Furthermore, as the twist approaches 90°, two channels establish, which transfer the electronic population from S_4 to S_2. By contrast, the oscillator strength of S_4 (0.09 a.u. in the twisted region) is connotative of a poor absorption, suggesting that the existence of an emissive path from S_4 is conditioned to the presence of a higher excited state, transferring its population to S_4 through a non-radiative channel. The steep increase of the Π index associated with the S_5 to S_4 decay at $\tau = 90°$ validates this hypothesis. Similar reasoning holds for S_5, whose population is maintained by S_6, which absorbs at 0° and approaches S_5 at 60°.

Close to $\tau = 90°$, all Π curves, except that computed for the S_3-S_1, S_2-S_1 and the S_1-S_0 interconversion visibly rise. This increase again points out the formation of several interconnected decay sub-channels (S_4-S_3, S_4-S_2, S_3-S_2,) enhancing the transfer of population from S_4 to S_2. Once more, these sub-channels are not necessarily driven by the energy gap, which ranges between 0.01 a.u. for S_4-S_2 and 0.003 a.u. for S_3-S_2. As such, the formation of these channels is supported by the similar distributions of the electronic densities of the states

involved, as witnessed by the small $q_{CT} \cdot D_{CT}$ values - computed Π values are reported in Supporting Information (*Table 4*).

Remarkably, the drop in the S_1-S_0 weighted-Π curve suggests the absence of the emission from S_1 (ICT_1) at 90°. Indeed, the orthogonality of the donor (dimethylaminophenyl) and acceptor (1,10-Phenanthroline) moieties hinders the formation of the ICT_1 state. As a consequence, the lowest emitting state at τ = 90° is S_2 (*LE*).

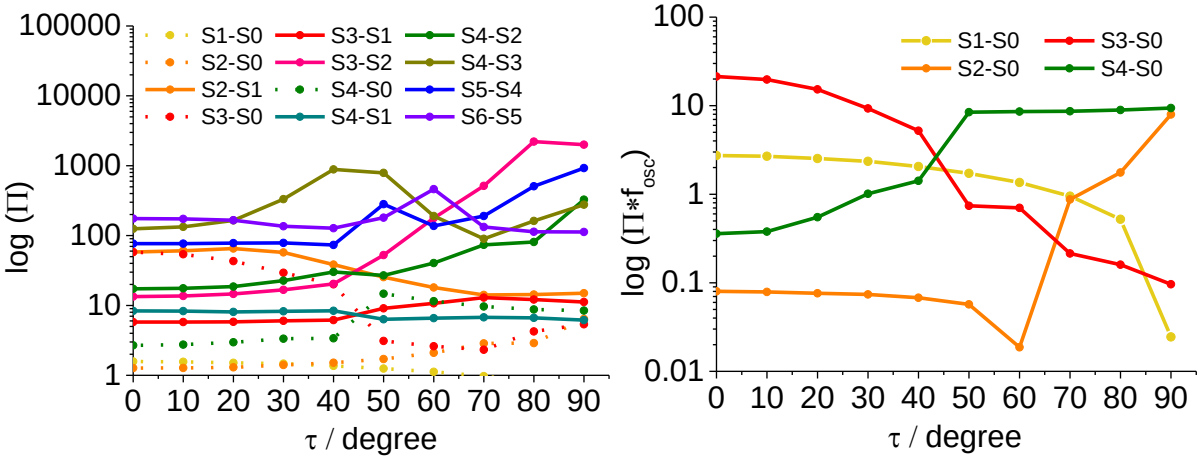

Figure 5 **(Left)** Evolution of Π index (in logarithm scale) along the reaction coordinated (the dihedral angle τ). **(Right)** The evolution of Π weighted by the oscillator strength (in logarithm scale).

In light of the discussion above, the dual emission mechanism observed in Phen-$PENMe_2$ can be summarized by the Jablonski diagram shown in *Figure 6*.

The population of the S1 - ICT_1 planar state in the FC region - leads to the ICT_1 emission experimentally observed at 560 nm[15]. Moreover, irradiation at a higher excitation wavelength allows reaching S_4. From S_4 a decay channel can open, leading to the population of S_2, a ππ* state of local character (*LE*). The relaxation through the vibrational sublevels of S_2 causes the observed fluorescence band observed at 421 nm in the experimental spectrum[15].

The S_4-S_0 curve suggests the existence of a further radiative decay at τ = 90 °. This channel is connected to S_6 - in the planar conformation. However, further internal deactivation channels between S_4-S_3 and S_3-S_2 can intervene, reducing the decay from S_4 and resulting in an enhanced S_2-S_0 emission. Similarly, S_3-S_1 and S_3-S_2 curves hint to the existence of two non-radiative channels which, in the planar conformation, contribute to impoverish the S_3-S_0 channel. All of the observable evidence leads to the conclusion that the emission from *LE* violates Kasha's rule. To explain this unusual behavior, it is instructive to examine the energy, and $q_{CT} \cdot D_{CT}$ values of the S_2-S_1 transition, at τ = 0 ° and τ = 90 °. At τ = 0° ΔE equals 0.021 a.u.. The $q_{CT} \cdot D_{CT}$ product is small (0.83 a.u.), which reflects a high similarity in the character of the two states. On the other hand, at 90°, while the energy gap shrinks to 0.007

a.u., $q_{CT} \cdot D_{CT}$ increases by one order of magnitude (9.07 a.u.). Although S_1 and S_2 are closer in energy at 90° than at 0°, the computed Π index is higher at 0°, reinforcing the hypothesis that a decay channel transfers the population from S_2 to S_1 at 0°, but not at 90°, allowing S_2 to emit radiatively.

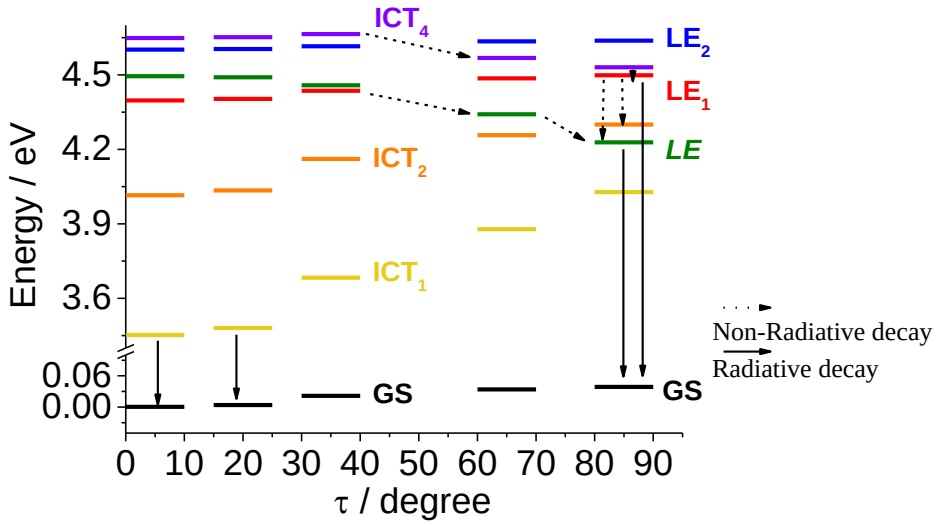

Figure 6 Jablonski Diagram describing the anti-Kasha dual emission of Phen-PENMe$_2$ molecule.

4. Conclusions

In summary, we have applied the index Π to unravel the excited state decay pathway of the Phen-PENMe$_2$ molecule. We have postulated the existence of different radiative and non-radiative decay pathways, related to structural reorganization occurring at the excited state, which bring to the formation of the observed dual emission.

Two factors are crucial when the interconversion between states is concerned. The closer in energy are the two states, the higher the likelihood that the interconversion occurs. On the other hand, the more similar the electronic densities of the two states, the higher the possibility of decay. The Π index includes both criteria in a single definition. The energy proximity of the two states is evaluated as the energy difference between two states, while the similarity between their electron densities is recovered through the product $q_{CT} \cdot D_{CT}$ - equivalent to the norm of the difference between their dipole moments.

Using the index Π, we could estimate the relative probabilities of different radiative and non-radiative channels, and infer a coherent picture of the decay pathways of the states involved in this photochemical process.

In particular, we have individuated two main radiative channels, which lead to the formation of two structurally different emissive species, a planar and a 90° twisted one. These findings

also agree with the outcomes of previous work.[15,16] Remarkably, our analysis points out the anti-Kasha mechanism of the LE emission. Besides, we have identified several sub-channels that play an essential role, enhancing either of the two emissions.

To conclude, the analysis that we have carried out shows the capability of the Π index to draw a qualitative map of a photochemical reaction. Although we have focused on one particular system, such analysis could be performed in a similar fashion to unveil the mechanism of other photochemical reactions of interest. Finally, in a more general perspective the present computational strategy may be particularly interesting for the rational design of substituted Phen-PENMe$_2$ derivatives with a targeted dual emission.

Supporting information

Tables containing optimized Cartesian coordinates of ten structures used, vertical excitation energies, $D_{CT,}$ oscillator strength and dipole moment data computed for each excited state. NTOs representation. Absorption energies and oscillator strength data used to calculate the UV-visible absorption spectrum. Energy differences, q_{CT}, D_{CT} and Π data computed for each excited state decay pathway.

Acknowledgments

This project has received funding from the European Research Council (ERC) under the European Union's Horizon 2020 research and innovation programme (grant agreement No 648558, STRIGES CoG grant).

Declaration of interest. There are no known conflicts of interest associated with this publication.

1 J. Chen, T. Yu, E. Ubba, Z. Xie, Z. Yang, Y. Zhang, S. Liu, J. Xu, M. P. Aldred and Z. Chi, *Advanced Optical Materials*, 2019, **115**, 1801593–7.

2 I. Marghad, F. Bencheikh, C. Wang, S. Manolikakes, A. Rérat, C. Gosmini, D. H. Kim, J.-C. Ribierre and C. Adachi, *RSC Adv.*, 2019, **9**, 4336–4343.

3 Q. Huang, X. Mei, Z. Xie, D. Wu, S. Yang, W. Gong, Z. Chi, Z. Lin and Q. Ling, *J. Mater. Chem. C*, 2019, **7**, 2530–2534.

4 B. Huang, W.-C. Chen, Z. Li, J. Zhang, W. Zhao, Y. Feng, B. Z. Tang and C.-S. Lee, *Angew. Chem. Int. Ed.*, 2018, **57**, 12473–12477.

5 Z. He, X. Cai, Z. Wang, D. Chen, Y. Li, H. Zhao, K. Liu, Y. Cao and S.-J. Su, *Sci. China Chem.*, 2018, **61**, 677–686.

6 P. L. dos Santos, M. K. Etherington and A. P. Monkman, *J. Mater. Chem. C*, 2018, **6**, 4842–4853.

7 W.-H. Chen, Y. Xing and Y. Pang, *Org. Lett.*, 2011, **13**, 1362–1365.

8 B. Liu, H. Wang, T. Wang, Y. Bao, F. Du, J. Tian, Q. Li and R. Bai, *Chem. Commun.*, 2012, **48**, 2867–2869.

9 U. Warde and S. Nagaiyan, *"Journal of Photochemistry & Photobiology, A: Chemistry,"* 2017, **337**, 33–43.

10 Y. Wu, X. Peng, J. Fan, S. Gao, M. Tian, A. J. Zhao and S. Sun, *J. Org. Chem.*, 2006, **72**, 62–70.

11 Y. Wu, X. Peng, J. Fan, S. Gao, M. Tian, J. Zhao and S. Sun, *J. Org. Chem.*, 2007, **72**, 62–70.

12 G. Ulrich, F. Nastasi, P. Retailleau, F. Puntoriero, R. Ziessel and S. Campagna, *Chem. Eur. J.*, 2008, **14**, 4381–4392.

13 U. Subuddhi, S. Haldar, S. Sankararaman and A. K. Mishra, *Photochem. Photobiol. Sci.*, 2006, **5**, 459–466.

14 S. Luber, K. Adamczyk, E. T. J. Nibbering and V. S. Batista, *J. Phys. Chem. A*, 2013, **117**, 5269–5279.

15 S. Chevreux, C. Allain, L. Wilbraham, K. Nakatani, P. Jacques, I. Ciofini and G. Lemercier, *Faraday Discuss.*, 2015, **185**, 285–297.

16 S. Chevreux, R. Paulino Neto, C. Allain, K. Nakatani, P. Jacques, I. Ciofini and G. Lemercier, *Physical Chemistry Chemical Physics*, 2015, **17**, 7639–7642.

17 L. Wilbraham, M. Savarese, N. Rega, C. Adamo and I. Ciofini, *J. Phys. Chem. B*, 2014, **119**, 2459–2466.

18 H. Tanaka, K. Shizu, H. Nakanotani and C. Adachi, *J. Phys. Chem. C*, 2014, **118**, 15985–15994.

19 N. Nagarajan, G. Velmurugan, P. Venuvanalingam and R. Renganathan, *"Journal of Photochemistry & Photobiology, A: Chemistry,"* 2014, **284**, 36–48.

20 S. Jana, S. Dalapati, S. Ghosh and N. Guchhait, *"Journal of Photochemistry & Photobiology, A: Chemistry,"* 2013, **261**, 31–40.

21 R. V. Pereira, A. P. Garcia Ferreira and M. H. Gehlen, *Excited-State Intramolecular Charge Transfer in 9-Aminoacridine Derivative*, American Chemical Society, 2005, vol. 109.

22 R. V. Pereira and M. H. Gehlen, *J. Phys. Chem. B*, 2006, **110**, 6537–6542.

23 M. K. Etherington, F. Franchello, J. Gibson, T. Northey, J. Santos, J. S. Ward, H. F. Higginbotham, P. Data, A. Kurowska, P. L. Dos Santos, D. R. Graves, A. S. Batsanov, F. B. Dias, M. R. Bryce, T. J. Penfold and A. P. Monkman, *Nat Commun*, 2017, **8**, 1–11.

24 M. Okazaki, Y. Takeda, P. Data, P. Pander, H. Higginbotham, A. P. Monkman and S. Minakata, *Chemical Science*, 2017, **8**, 2677–2686.

25 K. Wang, C.-J. Zheng, W. Liu, K. Liang, Y.-Z. Shi, S.-L. Tao, C.-S. Lee, X.-M. Ou and X.-H. Zhang, *Adv. Mater.*, 2017, **29**, 1701476–9.
26 J. C. Germino, C. A. Barboza, F. J. Quites, P. A. M. Vazquez and T. D. Z. Atvars, *J. Phys. Chem. C*, 2015, **119**, 27666–27675.
27 J. Sanz García, F. Maschietto, M. Campetella and I. Ciofini, *J. Phys. Chem. A*, 2017, **122**, 375–382.
28 M. Savarese, U. Raucci, P. A. Netti, C. Adamo, N. Rega and I. Ciofini, *Theoretical Chemistry Accounts*, 2016, **135**, 1–7.
29 M. Savarese, P. A. Netti, C. Adamo, N. Rega and I. Ciofini, *J. Phys. Chem. B*, 2013, **117**, 16165–16173.
30 P. Lutsyk, Y. Piryatinski, O. Kachkovsky, A. Verbitsky and A. Rozhin, *J. Phys. Chem. A*, 2017, **121**, 8236–8246.
31 B. F. E. Curchod, A. Sisto and T. J. Martínez, *J. Phys. Chem. A*, 2016, **121**, 265–276.
32 E. Titov, A. Humeniuk and R. Mitrić, *Physical Chemistry Chemical Physics*, 2018, **20**, 25995–26007.
33 M. Segado, E. Benassi and V. Barone, *J. Chem. Theory Comput.*, 2015, **11**, 4803–4813.
34 I. Gómez, P. J. Castro and M. Reguero, *J. Phys. Chem. A*, 2015, **119**, 1983–1995.
35 J. Catalán, *Physical Chemistry Chemical Physics*, 2013, **15**, 8811–10.
36 M. Barbatti, A. J. A. Aquino, H. Lischka, C. Schriever, S. Lochbrunner and E. Riedle, *Physical Chemistry Chemical Physics*, 2009, **11**, 1406–1415.
37 M. Savarese, É. Brémond, C. Adamo, N. Rega and I. Ciofini, *Chemphyschem*, 2016, **17**, 1530–1538.
38 U. Raucci, M. Savarese, C. Adamo, I. Ciofini and N. Rega, *J. Phys. Chem. B*, 2015, **119**, 2650–2657.
39 M. Savarese, U. Raucci, C. Adamo, P. A. Netti, I. Ciofini and N. Rega, *Physical Chemistry Chemical Physics*, 2014, **16**, 20681–20688.
40 S. A. Mewes and A. Dreuw, *Physical Chemistry Chemical Physics*, 2019, **21**, 2843–2856.
41 F. Maschietto, M. Campetella, M. J. Frisch, G. Scalmani, C. Adamo and I. Ciofini, *J. Comput. Chem.*, 2018, **39**, 735–742.
42 T. Le Bahers, C. Adamo and I. Ciofini, *J. Chem. Theory Comput.*, 2011, **7**, 2498–2506.
43 M. Campetella, A. Perfetto and I. Ciofini, *Chem. Phys Lett*, 2019, **714**,81–86.
44 M. Campetella, F. Maschietto, M. J. Frisch, G. Scalmani, I. Ciofini and C. Adamo, *J. Comput. Chem.*, 2017, **38**, 2151–2156.
45 F. Maschietto, J. Sanz García, M. Campetella and I. Ciofini, *J. Comput. Chem.*, 2019,**40**, 650–656.
46 E. Lippert, W. Lüder, F. Moll, W. Nägele, H. Boos, H. Prigge and I. Seibold-Blankenstein, *Angew. Chem.*, 1961, **73**, 695–706.
47 C. Huang, X. Peng, D. Yi, J. Qu and H. Niu, *Sensors and Actuators B: Chemical*, 2013, **182**, 521–529.
48 M. E. Casida, C. Jamorski, K. C. Casida and D. R. Salahub, 1998, **108**, 4439–4449.
49 F. Furche and R. Ahlrichs, *J Chem Phys*, 2002, **117**, 7433–7447.
50 T. Yanai, D. P. Tew and N. C. Handy, 2004, **393**, 51–57.
51 M. M. Francl, W. J. Pietro, W. J. Hehre, J. S. Binkley, M. S. Gordon, D. J. DeFrees and J. A. Pople, *The Journal of Chemical Physics*, 1982, **77**, 3654–3665.
52 P. Wiggins, J. A. G. Williams, D. J. Tozer *J. Chem. Phys.* 2009, **131**, 091101
53 C. A. Guido, B. Mennucci, D. Jacquemin, C. Adamo *Phys. Chem. Chem. Phys.* 2010,**12**, 8016-8023

54 V. Barone and M. Cossi, *J. Phys. Chem. A*, 1998, **102**, 1995–2001.
55 C. A. Guido, D. Jacquemin, C. Adamo, B. Mennucci *J. Chem. Theory Comput.*2015, **11**, 5782-5790
56 Gaussian 16, Revision B.01, M. J. Frisch, G. W. Trucks, H. B. Schlegel, G. E. Scuseria, M. A. Robb, J. R. Cheeseman, G. Scalmani, V. Barone, G. A. Petersson, H. Nakatsuji, X. Li, M. Caricato, A. V. Marenich, J. Bloino, B. G. Janesko, R. Gomperts, B. Mennucci, H. P. Hratchian, J. V. Ortiz, A. F. Izmaylov, J. L. Sonnenberg, D. Williams-Young, F. Ding, F. Lipparini, F. Egidi, J. Goings, B. Peng, A. Petrone, T. Henderson, D. Ranasinghe, V. G. Zakrzewski, J. Gao, N. Rega, G. Zheng, W. Liang, M. Hada, M. Ehara, K. Toyota, R. Fukuda, J. Hasegawa, M. Ishida, T. Nakajima, Y. Honda, O. Kitao, H. Nakai, T. Vreven, K. Throssell, J. A. Montgomery, Jr., J. E. Peralta, F. Ogliaro, M. J. Bearpark, J. J. Heyd, E. N. Brothers, K. N. Kudin, V. N. Staroverov, T. A. Keith, R. Kobayashi, J. Normand, K. Raghavachari, A. P. Rendell, J. C. Burant, S. S. Iyengar, J. Tomasi, M. Cossi, J. M. Millam, M. Klene, C. Adamo, R. Cammi, J. W. Ochterski, R. L. Martin, K. Morokuma, O. Farkas, J. B. Foresman, and D. J. Fox, Gaussian, Inc., Wallingford CT, 2016.
57 CTM Group, *http://www.quanthic.fr*.
58 J. C. Sancho-García and A. J. Pérez-Jiménez, *J. Chem. Phys.* 2003, **119**, 5121–5127.